Multiscale Modelling of $Cu_xAg_yAu_{1-x-y}$ surface segregation for propylene epoxidation

Ankit Kumar Gautam

Submitted in partial fulfillment of the requirements for the degree of

Master of Science

Department of Chemical Engineering

Carnegie Mellon University

Pittsburgh, PA, USA

November 23, 2020

Contents

Abstract

Multicomponent alloys very often exhibit superior properties than their constituent individual metals. For an industrially relevant reaction such as propylene epoxidation, an appropriate catalyst can greatly enhance the selectivity and conversion of the process. For example, Ag based catalysts show excellent activity but alloying Ag with Cu or Au exhibit increased selectivity and conversion. We postulate that there exists an alloy of composition $Cu_xAg_yAu_{1-x-y}$ which posseses desired target property or some combination of those properties. In the pursuit of finding this optimum composition, one needs to be aware of effects of the phenomenon of surface segregation which states that the surface composition of a multicomponent alloy often differs from its bulk composition. This deviation depends on bulk concentrations, temperature, pressure and adsorbates present on surface. This study is focussed on understanding the extent of surface segregation on all possible compositions in $Cu_xAg_yAu_{1-x-y}$ ternary system. Fast computational methods allow us to accurately predict the changes due to surface segregation for any given bulk composition. In this work, surface segregation is modelled via Monte Carlo simulations in canonical ensemble. To evaluate energies of intermediate configurations arising during Monte Carlo simulations, a machine learning model is trained on first principles Density Functional Theory (DFT) energies. Combination of these computational tools lets us predict the deviation of surface composition from bulk composition of a multicomponent alloy.

Keywords: Density Functional Theory, Neural Network, Multiscale Modelling, Surface Segregation, Monte Carlo, Ternary Phase Diagram

List of Figures

List of Tables

1 Introduction

1.1 Surface segregation

Surface segregation is the phenomena of preferential enrichment of one specie within a multicomponent alloy. Because of this, the surface composition of a catalyst often differs from its bulk composition. Many factors go into determining this deviation such as bulk composition, crystal facet, temperature and pressure of the system[1] or even the presence of an adsorbate on the surface.[2–4] The ability to quantify surface composition provides understanding of the underlying catalytic process. Pioneering work by McLean in 1957 for segregation in grain boundaries[5] is still used towards modelling segregation on surfaces. For the case of a binary metal alloy, the equation goes like

$$\frac{x_1^s}{1-x_1^s} = \frac{x_1^b}{1-x_1^b} exp\Big(-\frac{\Delta G_{seg}^{(1)}}{RT}\Big) \tag{1}$$

x_i^s in Eqn.1 denotes surface composition (mole fraction) of component i and x_i^b represents its bulk composition. $\Delta G_{seg}^{(i)}$ in all of these equations represents free energy change related to segregation of component i to the surface for one mole of atoms. T is the temperature in Kelvin. And the equations can be extended to a ternary case as follows:

$$\frac{x_1^s}{1-x_1^s-x_2^s} = \frac{x_1^b}{1-x_1^b-x_2^b} exp\Big(-\frac{\Delta G_{seg}^{(1)}}{RT}\Big) \tag{2}$$

$$\frac{x_2^s}{1-x_1^s-x_2^s} = \frac{x_2^b}{1-x_1^b-x_2^b} exp\Big(-\frac{\Delta G_{seg}^{(2)}}{RT}\Big) \tag{3}$$

In these equations, $\Delta G_{seg}^{(i)}$ is the big unknown that goes into the equations currently as the two non-linear equations can be readily solved together.

Efforts to model ternary segregation energy started with Hoffmann and co-workers[6] using regular solution nearest neighbor bond model.[7] Their work on dilute ternary systems viewed ternary systems as deviations from binary

system.[8,9] They also shed light on phenomena such as "cosegregation" and "site competition" useful for ternary segregation. Cosegregation occurs when the attractive forces from two surface active (having tendency to segregate) enrich surface together. Whereas site competition is observed when both surface active solutes have large enough concentrations capable of flooding the surface but clearly there is a maximum amount of total surface entities. Moreover, ternary segregation is not directly observed as binary segregation between the two surface active components, as Good et al.[10] also remarked from their results of CuAuNi ternary system. Good's work showed that in binary cases, Au and Cu segregate in Au-Ni and Cu-Ni system respectively and Au segregates in Au-Cu system. But, this knowledge cannot be extrapolated to conclude that Au would be the dominant surface component. Ternary interaction is much more complex than what one expects to be.[11]

Ternary surface segregation is often modeled as surface active species being solutes in a solvent. Because of such *impurities* various strain effects evolve to drive surface active species towards surface to obtain thermodynamically more stable structure. The segregation energy model called 'Atom Exchange Method' has been used in different forms over the years starting from Mclean,[5] Defay et. al.,[12] Wynblatt and Ku[11] and others. Most recent development by Zhao and co-workers[13,14] is explained and replicated later in this work.

1.2 Segregation in Cu, Ag, Au ternary alloys

We focus our study on design of catalyst intended for propylene epoxidation. Propylene oxide (PO) is a heavily used intermediate in the chemical industry. PO is produced from oxidation of propylene. At present the two dominant methods of productions are chlorohydrin process and hydroperoxide process. Both of the processes suffer from disadvantages such as use of expensive Cl_2 in the former and safety issues in the latter. A relatively new process

of direct epoxidation is of more interest to researchers because of improved productivity.

Silver rich catalysts have long been in use for the oxidation of alcohol[15] but they suffer from selectivity for epoxidation.[16,17] This occurs because the route of production moves towards undesirable Carbon-dioxide (total oxidation).[18] High selectivities have been observed by Ag addition on supported Cu catalysts,[19,20] Au addition onto TS-1 support,[21,22] and AuAg bimetallic catalyst.[23] This naturally raises the possibility of presence of a ternary system with both improved selectivity and conversion. This approach would require one to enumerate all possible combinations and then choose the best candidate among them. Copper, Silver and Gold also have convenient properties of having FCC bulk structures, do not form intermetallic compounds.[8] Moreover, these metals have been studied extensively over the years. Some properties relevant to surface of these metals are compiled in Tab.1

Table 1: Important properties of Copper, Silver and Gold

Material Properties	Cu	Ag	Au
Crystal structure[24]	FCC	FCC	FCC
$\gamma_{s,111}$ (J/m^2)[25]	1.952	1.172	1.283
Atomic Radius (pm)[24]	117	134	134
Electronic affinity (eV)[24]	1.24	1.30	2.31

1.3 Monte Carlo simulations to model surface segregation

To the best of our knowledge, no current work is present explicitly measuring CuAgAu segregation across all ternary space. Experimental work by Hoffmann et al.[8] represent only dilute values with Ag and Au composition less than 6%. Bozzolo–Ferrante–Smith (BFS) method[26] has been used to study CuAgAu through a mean field approach by fitting experimental properties of the binary systems is also used for dilute compositions.

First principles Density Functional Theory (DFT) provides increased accuracy when compared to other techniques such as Embedded Atom Method

(EAM), ReaxFF although at a cost of computational expense. Fortunately, this hindrance has been growing smaller with more advancements in computational techniques including that of machine learning and artificial intelligence.

It has been shown that a machine learning can be applied to capture the underlying high dimensional potential energy surface.[27,28] This allows us to use results comparable to DFT without conducting a DFT calculation. This idea of using a surrogate model of DFT brings down the computational cost up to 5 orders of magnitude.[28,29] Such a drastic reduction is partially achieved by implementing a cutoff radius to neglect faraway interactions. Specifically, we utilize Behler-Parinello Neural Network (BPNN) framework trained on DFT data. This procedure has been validated for the Au,[30,31] Cu,[32–34] and Ag.[35,36] This review by Prof. Behler[37] provides a comprehensive list of other materials also modeled using BPNN. Finally, this NN is used to quickly predict energies encountered within MC simulation, ultimately used to obtain surface compositions.

This work studies surface segregation by carrying out Monte Carlo (MC) simulations in a canonical ensemble utilizing a machine learned potential trained on DFT calculations. 4000+ DFT calculations were performed to cover the entire composition and configuration space. A Neural Network with 2 hidden layers and 10 nodes in each layer is trained on the DFT data. The Neural Network easily achieves the desired accuracy and demonstrates a similar Mean Absolute Error (MAE) on validation and test data. MC simulations were carried out for 20000 successful swaps to equilibrate the bulk and surface interaction. Surface excess plots were generated to survey surface segregation at various point of ternary space. Using the surface and bulk compositions, segregation energy at all compositions were evaluated using the Langmuir-Mclean equations as given in Eqn. 2.

2 Methods

2.1 Github repository

The code required to fully reproduce the results of this work is made available at https://github.com/gautamankitkumar/ankitgau-ms-report-data. The repository contains python code in Jupyter notebooks with detailed comments. The links at the top of each notebooks contains a hyperlink to Google Colab which executes python code on the cloud thus requiring no installation (including python) on the reader's computer.

2.2 DFT calculations

Density Functional Theory calculations were performed using the Vienna *ab initio* simulation package (VASP)[38–40] with the PerdewBurkeErnzerhof Generalized Gradient Approximation (GGA-PBE)[41,42] exchange-correlation functional. Core electrons were described using the projector augmented wave (PAW) potentials.[43,44] MonkhorstPack k-point grids[45] were chosen to have minimum 450 per reciprocal atom and planewave cutoff of 400 eV was selected. These settings give out a convergence error of below 1 meV/atom when comparing difference in energies.

Different sized slabs are created as follows:

- 100 of $1 \times 1 \times 7$,
- 100 of $2 \times 1 \times 7$,
- 200 of $\sqrt{3} \times \sqrt{3} \times 7$,
- 200 of $\sqrt{7} \times \sqrt{7} \times 5$ and,
- 200 of $3 \times 3 \times 5$

were generated at 5 lattice constants varying between smallest (Cu, 3.63 Å) and largest (Au, 4.17 Å) so that the Neural Network learns to capture the

underlying potential energy surface at different lattice constants. This totals to 4000 training data which would be fed into the Neural Network.

Various types of van der waals corrections to Perdew-Burke-Ernzerhof exchange-correlation functional (PBE) are tested for Ag-Au binary segregation. These include DFT-D2 proposed by Grimme et al.,[46] DFT-D3,[47] and Bayesian Error Estimation Functional with van der waals (BEEF–vdW).[48] The above mentioned corrections were easily implemented in Vasp by setting `ivdw` parameter to corresponding values.

2.3 Neural Network setup

Since DFT calculations are computationally expensive, a surrogate machine learning model is built to predict energy of an unknown configuration. To this end, a Behler Parinello Neural Network framework (BPNN)[28] was used to obtain energies of the surface slabs, where slabs are first transformed to fingerprints space through G^2 symmetry functions.[49] These symmetry functions work very well to capture the atomic environment around an atom. Information of chemical identities and positions of each atom is encoded within the symmetry functions. Such a transformation is necessary to make the energy model invariant to translation, rotation, permutation of atoms. G^2 values uses a cutoff function to remove interaction of faraway atoms. A cutoff function $f_c(R_{ij})$ where R_{ij} is the distance between atom i and atom j is defined as follows:

$$f_c(R_{ij}) = \begin{cases} 0.5 \times \left[\cos\left(\frac{\pi R_{ij}}{R_c}\right) + 1\right] & \text{for} R_{ij} \leq R_c \\ 0 & \text{for} R_{ij} > R_c \end{cases} \tag{4}$$

A `cosine` function is applied to exploit the smooth decay to value of zero at $r = R_c$. A single NN is trained for each distinct chemical species, in this case, each one for Cu, Ag, and Au. G^1 and G^2 for an element with atomic

number Z centered at atom i is written as follows

$$G_i^{1,Z} = \sum_j^Z f_c(R_{ij}) \tag{5}$$

$$G_i^{2,Z} = \sum_j^Z e^{-\eta(R_{ij}-R_s)^2} f_c(R_{ij}) \tag{6}$$

where the sum for j goes over for all atoms with atomic number Z which only accounts for atoms present inside a cutoff sphere. η, R_s are user defined hyperparameters which are fixed for values of $\eta = 0.05, 4, 20, 80$ and $R_s = 0$ for each η in this work. The role of η and R_s is to give different values for same input of R_{ij}. This vector of 4 values of symmetry functions is unique for each structure and avoids the problem of same energy for different configuration.[49] Cutoff radius is set as $R_c = 6$Å for each symmetry function as they work well for chosen metal species.[31,32]

For our case of three species the final input vector to Neural Network has a 12×1 shape containing the following quantities as enumerated in Tab. 2 There exists many other descriptors to represent an atomic environment

Table 2: Input Vector for Neural Network

Cu	G^2 for $\eta = 0.05$, $R_s = 0$ G^2 for $\eta = 4$, $R_s = 0$ G^2 for $\eta = 20$, $R_s = 0$ G^2 for $\eta = 80$, $R_s = 0$
Ag	G^2 for $\eta = 0.05$, $R_s = 0$ G^2 for $\eta = 4$, $R_s = 0$ G^2 for $\eta = 20$, $R_s = 0$ G^2 for $\eta = 80$, $R_s = 0$
Au	G^2 for $\eta = 0.05$, $R_s = 0$ G^2 for $\eta = 4$, $R_s = 0$ G^2 for $\eta = 20$, $R_s = 0$ G^2 for $\eta = 80$, $R_s = 0$

including the Coulomb Matrix,[50] Ewald sum Matrix,[51] Sine Matrix,[51] Many Body Tensor Representation,[52] Smooth Overlap of Atomic Orbitals.[53] A very

nice compilation of these descriptors is available in Himanen's work[54] and maintained online as a plug and play model as a python package.

All the NNs have the same architecture of 2 hidden layers with 10 hidden nodes each. Training is done over 80% of the data and 20% is left as validation and test data. The learning rate is set to be equal to 0.1 and the convergence criteria is set to achieve Mean Absolute Error of 2 meV/atom for the NN. No force training is carried out as we are only interested on energy prediction.

The training is conducted in a code written in Pytorch[55] and atomic simulation environment(ase).[56,57]

2.4 MC canonical ensemble procedure

Metropolis Monte Carlo simulations was performed with starting compositions spread throughout the ternary space. 20000 successful atomic swaps are carried out in a single simulation. A slab size of $10 \times 10 \times 15$ is used at temperature of 600 K. An atom and one of its (different specie) neighbor is chosen randomly at each of time step for a potential swap. Energy for the two structures, the original and one evolving because of the swap, is predicted using the trained NN. A successful swap is is considered when total energy is lowered due to the swap. A swap is also accepted by Boltzmann probability criteria. Full algorithm is described in Algorithm 1.

Algorithm 1: Monte Carlo algorithm

Result: Equilibrium Surface composition

Input

T : Temperature in Kelvin

X_{Cu}, X_{Ag}, X_{Au} : Starting compositions for each element

Initialize Successful_Steps = 0;

while *Successful_Steps* ≤ 20000 **do**

$Atom1 \leftarrow SelectAtomAtRandom()$

$Atom2 \leftarrow SelectAtom1'sNeighbor()$ *//Different Specie*

Temp_Configuration $\leftarrow$ *Switch Atom1 and Atom2*

$E\_1 \leftarrow Energy(Original\_Configuration)$

$E\_2 \leftarrow Energy(Temp\_Configuration)$

$\Delta E \leftarrow E_2 - E_1$

$h \leftarrow Random(0, 1)$ $//UniformRandomNumber$

if $\Delta E \leq 0$ *or* $h \leq exp\Big(-\frac{\Delta E}{k_B T}\Big)$ **then**

Update Successful_Steps+=1;

$Original\_Configuration \leftarrow Temp\_Configuration$ **end**

end

This algorithm describes the state of entire slab at each iteration and its composition (including layer-by-layer) information is recorded at 100 step intervals. Using the average of last 40 values, the final state of the slab is obtained and surface excess (final-initial composition) plotted at each data point.

3 Results and Discussion

3.1 Include *k* point and encut convergence plots

Need to make a GitHub repo with all the results into a python notebook

3.2 Include ternary diagram and fingerprint space

DFT calculations on slabs with sizes as mentioned in 2.2 are carried out with randomized compositions. Dirichlet sampling is used to generate the sampling points. The sampled compositions are plotted as follows in Fig 1

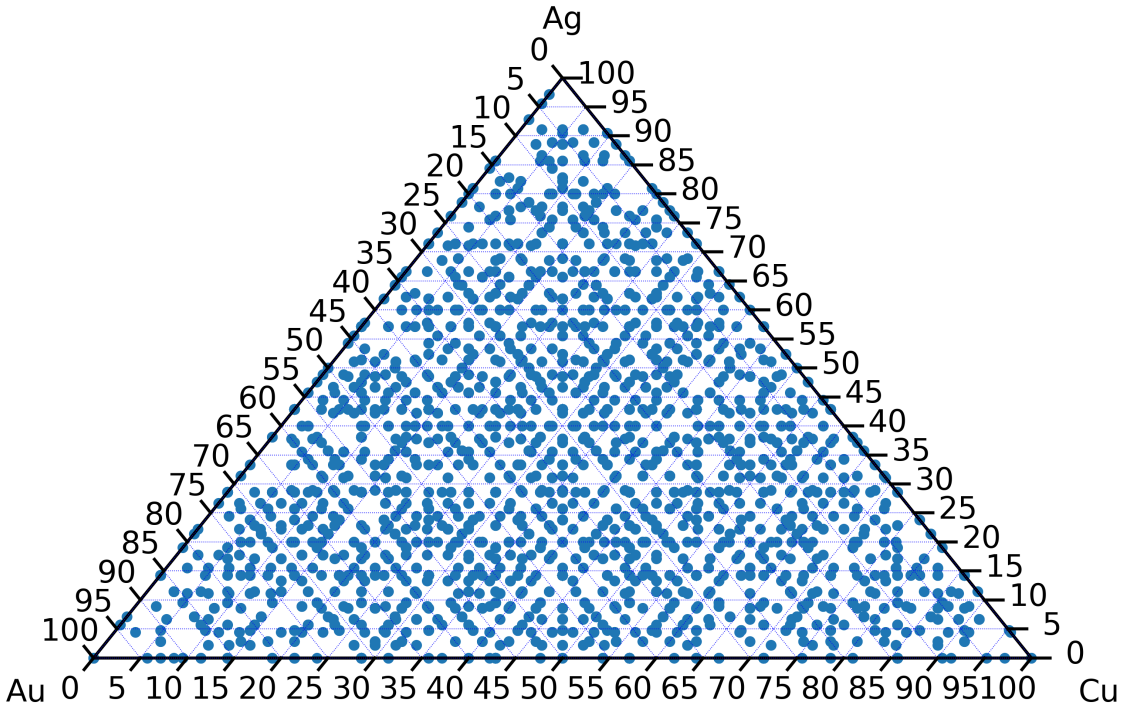

Figure 1: 4000 sampled compositions across ternary space

And since these points would go into the Neural Network input space, the fingerprint space is also plotted in Fig 2.

These two plots show that the chosen composition points cover the ternary space entirely.

3.3 Neural Network Training

NN training is conducted on 80% of the data with a convergence criteria of Mean Absolute Error (MAE) of 2 meV/atom. Validation and test data is separated from training data to provide the measure of performance of NN on unseen data. The Neural Network performs very well and achieves almost

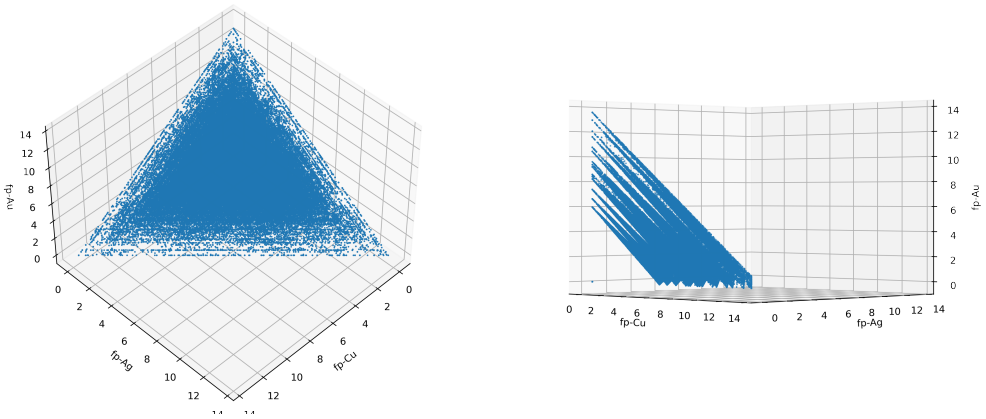

Figure 2: Fingerprint space of the 4000 data points

similar MAE on unseen data. NN accuracy is not affected much when any of the parameters such as NN architecture, learning rate, number of epochs is changed. NN training on the data is summarized in Fig. 3.

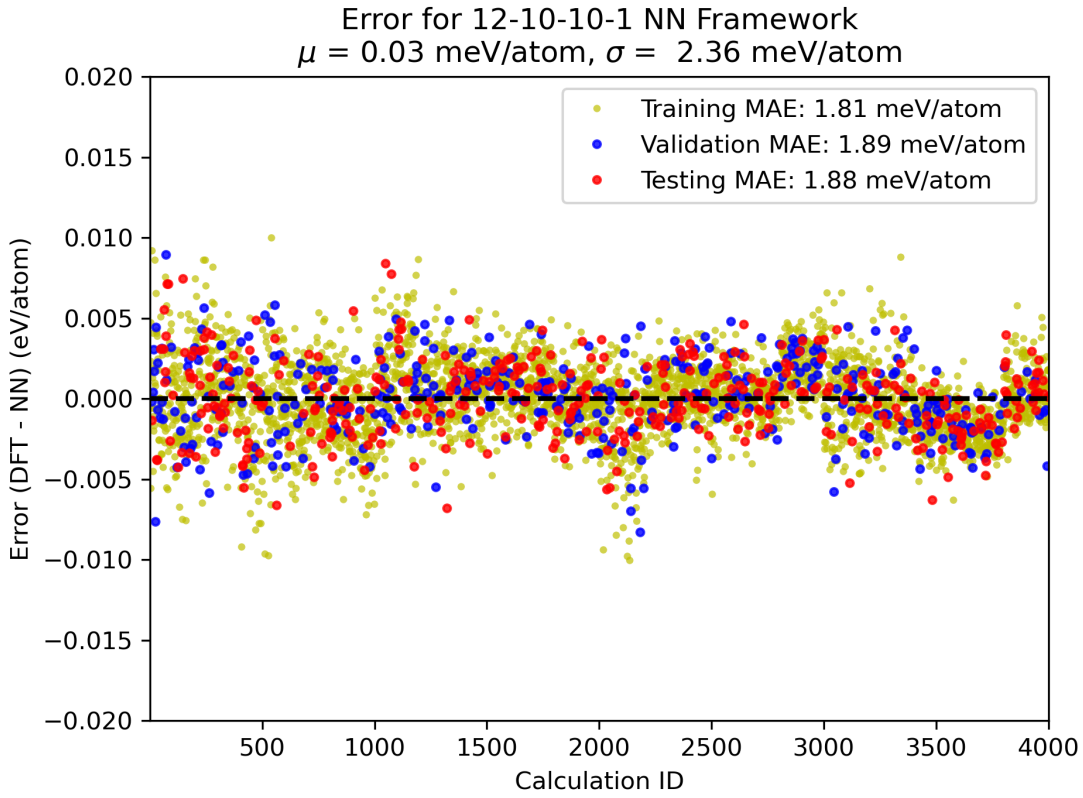

Figure 3: NN performance and training data.

The trend in the MAE occurs partly occurs only because the training data

itself is structured. The standard deviation of 2.5 meV/atom shows that the spread around zero is very small when compared to segregation energies.

3.4 Monte Carlo simulations

Monte Carlo simulations are carried out at composition intervals of 10%, i.e. (0,10,90), (0,20,80) and so on. Simulations are carried out for 20000 steps which is chosen as the time when all the favorable swaps have already occurred and equilibrium is achieved. This sampling on compositions is dense enough to capture the underlying surface excess trend. To aid the visualization process, an interactive graph in plotly[58] is created in jupyter notebooks. When a user clicks on a point in Fig. 4, a plot is generated as seen in Fig. 5, which is the desired Monte Carlo trajectory.

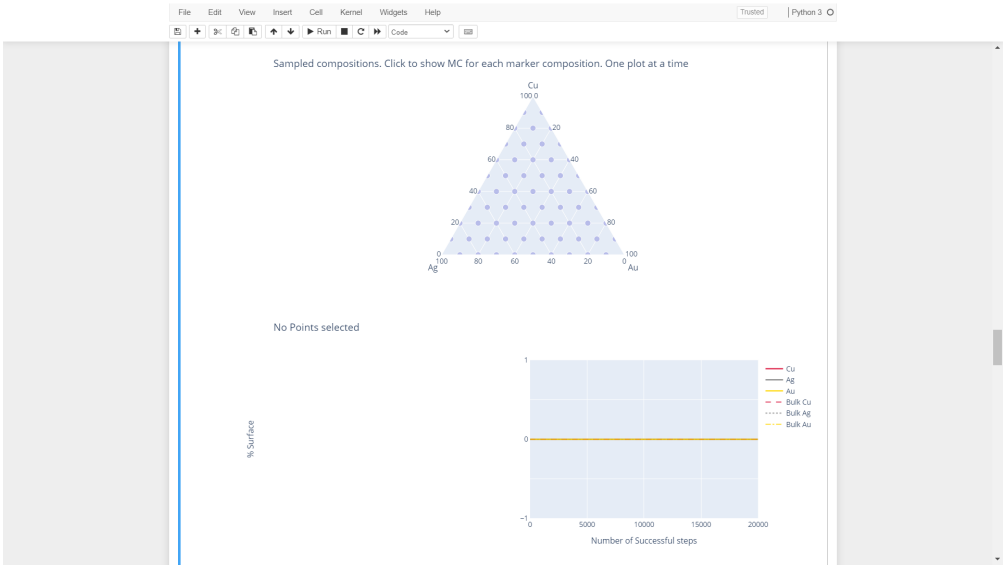

Figure 4: Screenshot of Jupyter notebook before click

A single sample image from for a clicked image is shown in Fig. 6. Notice how in this given case, gold surface composition shoots up and copper surface composition goes down. This composition shows a case of gold segregation to the surface and copper dissolution into the bulk.

Surface excess is calculated as difference between the final composition

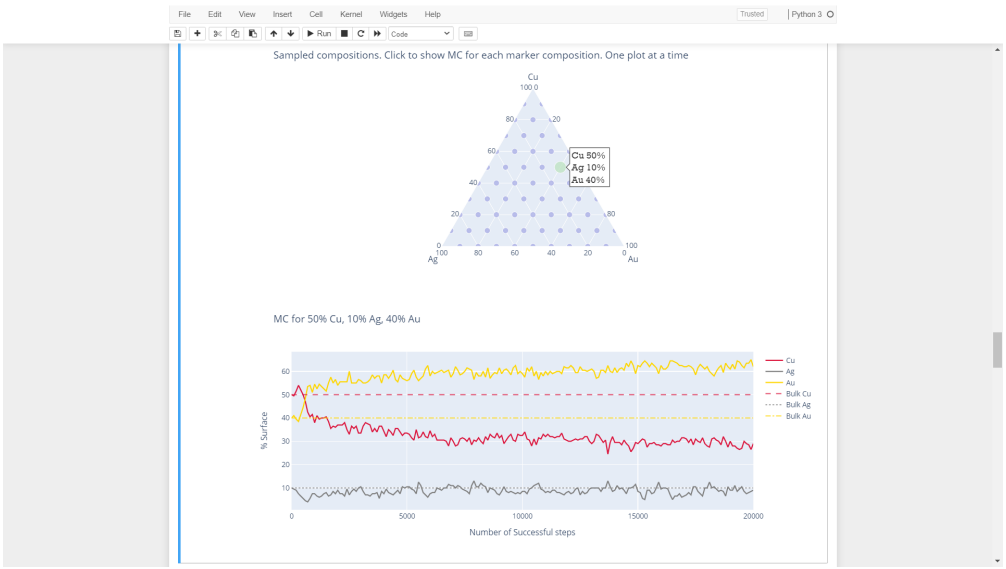

Figure 5: After click on a composition point

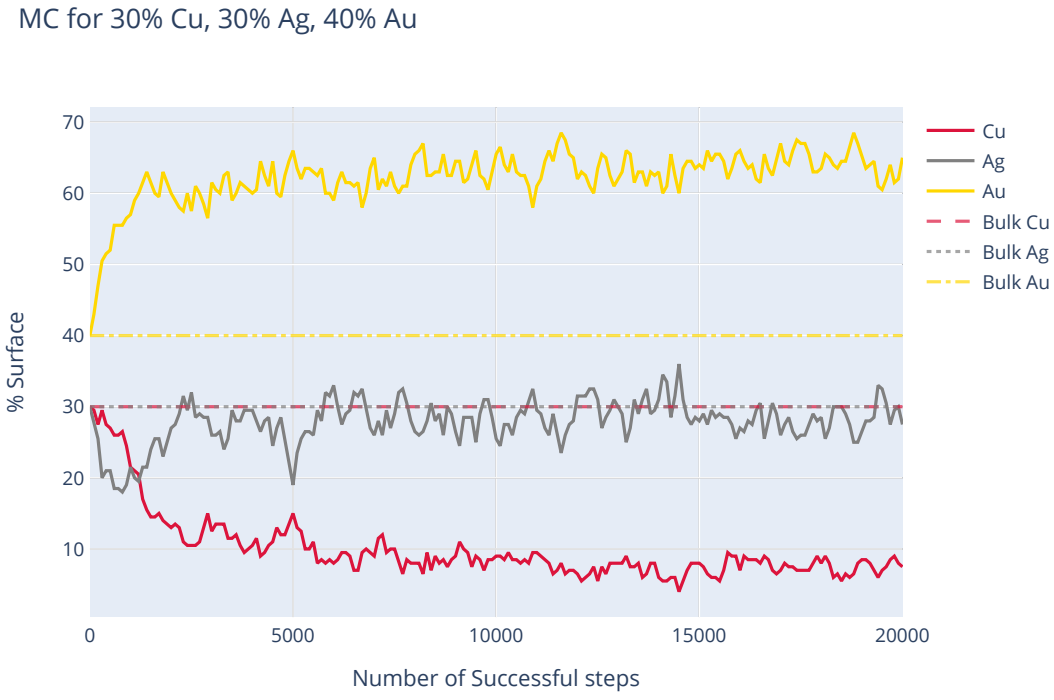

Figure 6: Surface composition trajectory for 30% Cu, 30% Ag, 40% Au

and initial composition for each point. The initial composition of the surface is equal to the bulk composition of the composition of interest. The final composition is taken as average of last 40 values i.e. time steps 16000 to 20000. This gives a discrete set of values of each element on each sampled point within the ternary diagram. The contour plots are generated used `matplotlib`'s `tricontour` and `tricontourf` functions. The obtained surface excess are shown in Fig. 7.

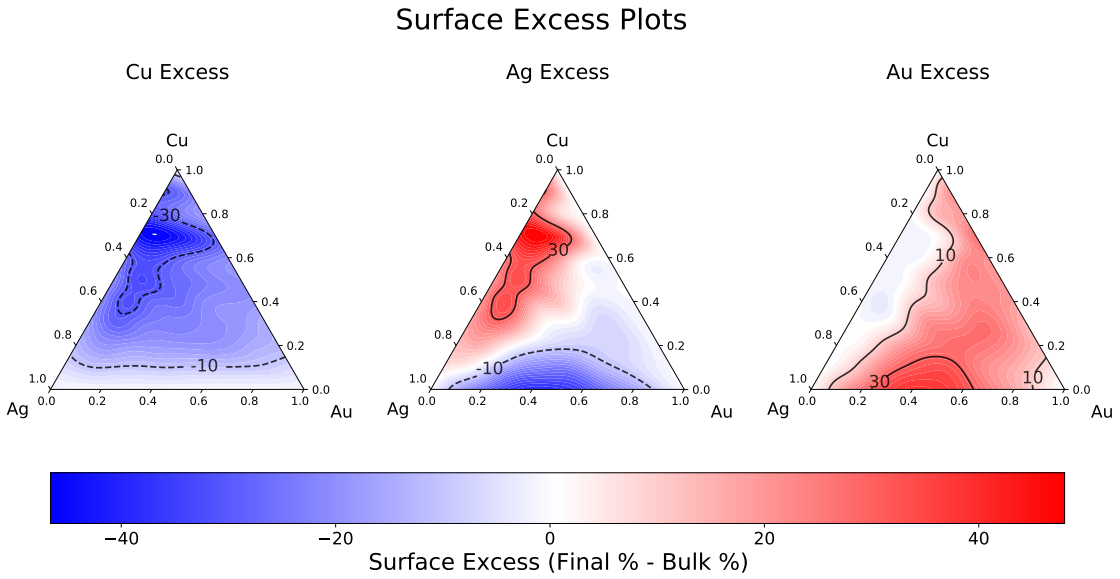

Figure 7: Monte Carlo Surface Excess Plot

One reads the above plot by selecting a point on the ternary phase diagram, which fixes the initial surface composition and then matching the color observed at that point with the color scale drawn at the bottom. Wikipedia has an excellent guide to read values from a ternary plot. Now, the three plots give excess values for the three species i.e Cu, Ag and Au. For the case of copper excess (leftmost), picking almost any point is blue-colored which means that our model predicts copper to move into bulk and reduce its composition from its initial composition.

3.5 Discussion on surface excess values

To justify the results obtained, understanding on segregation phenomena is important. Segregation energy (and thus the segregation behavior) stems from mainly these three main contributions as per atom-exchange method.[6] These are:

1. Difference in surface energies,
2. Mixing behavior of the participating metals and,
3. Solute elastic strain

Treglia et. al.[59] remarks that segregation in 95% of bimetallic systems can be explained solely by the first contribution of difference in surface energies. The rest 5% is constituted by cases where a huge size difference exists between the elements. From surface energies mentioned in Tab. 1, copper mixing into the bulk is correctly predicted when present in a mixture either gold or silver. Copper dissolution into the bulk is also observed over the years, both experimentally,[8,14,60,61] and computationally.[62–64]

Silver segregation in copper rich regions is correctly predicted (similar argument as above) but silver dissolution in gold rich areas is contradictory to what is observed experimentally. This discrepancy is further explored in a subsequent section in more detail.

Gold segregation in copper rich regions is rightly predicted also observed experimentally[8,65–67] and computationally[9,62]

3.6 Segregation energies for binary pairs from McLean equations

Assuming the segregation behavior as three binary surface segregation occurring together, the following three equations can be written:

$$\mathrm{Cu_{bulk} + Ag_{surf} \leftrightharpoons Cu_{surf} + Ag_{bulk}} \qquad \mathrm{K_{CuAg}} = \frac{\mathrm{y_{Cu}x_{Ag}}}{\mathrm{y_{Ag}x_{Cu}}} \tag{7}$$

$$\mathrm{Ag_{bulk} + Au_{surf} \leftrightharpoons Ag_{surf} + Au_{bulk}} \qquad \mathrm{K_{AgAu}} = \frac{\mathrm{y_{Ag}x_{Au}}}{\mathrm{y_{Au}x_{Ag}}} \tag{8}$$

$$\mathrm{Au_{bulk} + Cu_{surf} \leftrightharpoons Au_{surf} + Cu_{bulk}} \qquad \mathrm{K_{AuCu}} = \frac{\mathrm{y_{Au}x_{Cu}}}{\mathrm{y_{Cu}x_{Au}}} \tag{9}$$

where x denotes bulk (initial) composition and y represents final surface composition (fraction). The ordering of elements is kept such that when combined together, the equilibrium constants can be multiplied to unity.

$$\mathrm{K_{CuAg}K_{AgAu}K_{AuCu}} = 1$$

x and y in Eqn. 7 are readily obtained from the Monte Carlo data and thus, utilized to calculate equilibrium constants for each case. Within each case, only data points where the composition of each individual component is no less than 20% is taken to avoid numerical instabilities in calculating equilibrium constants. For a case of an example pair of metals A and B, segregation free energy is then calculated using $\Delta G_{seg,AB} = -RTln(K_{AB})$. Using R as $8.314\frac{J}{molK}$ and $T = 600K$, we get segregation energy across the ternary space. The plot is available at Fig. 8.

The segregation energy values calculated here are roughly in the same order of magnitude as those reported earlier in literature. CuAg segregation energy is reported as 0.22 eV/atom[62] which is roughly 21.2 kJ/mol. Fig 8 shows values ranging from 0 to 15 kJ/mol. We observe AgAu segregation energies in the range 0 to 7 kJ/mol while it is reported as 0.00 eV/atom and classified as mild or no segregation. Not only is the value incorrect but the segregation trend is not what is observed experimentally. AuCu segregation is seen as always negative and varies from -5 to -15 kJ/mol and it is described as -0.29 eV/atom[62] which becomes -28 kJ/mol. The segregation trend of CuAg

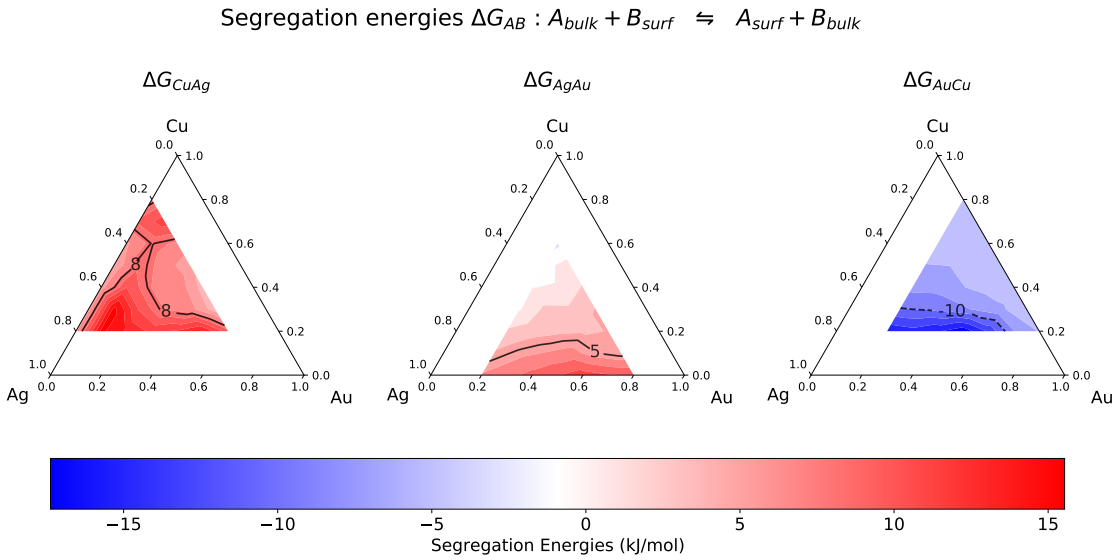

Figure 8: Segregation Free Energy at Ternary Compositions

and AuCu is obtained correctly while for AgAu case it appears contrasting to previously known values. More discussion on AgAu segregation takes place in subsequent section.

3.7 Dispersion force contribution to AgAu segregation

As seen in the previous two sections, among AgAu binary pair, Au is predicted to segregate to the surface. This is directly in contrast to the surface energies values described in Tab. 1 which predicts Ag segregation because of its lower surface energies. Various experimental studies report zero[68,69] and moderate Ag segregation.[70–75] But, on the other hand, computational methods predict Ag segregation[76,77] and also Au segregation.[78–81]

It has been suggested that for these two metals that the surface properties are dependent on correctly including van der waals (vdw) forces by a study by Rehr et. al.[82] The authors explain how polarization forces contribute upto 14% and 17% to cohesive energies of Ag and Au respectively.

Dispersion forces or it is also called long ranged forces are present everywhere. Although weak in nature, they are important features to some se-

lective problems. Various dispersion corrections to DFT energies have been suggested over the years with most of it gaining popularity in last couple of decades.[83] Klimes et. al. provide a great summary of different versions (complexity) of vdw corrections that have been employed to better predict properties such as adsorption energy or binding energy among many others. In the most simplest form, vdw corrections take the form of following equations:

$$E_{\text{tot}} = E_{\text{DFT}} + E_{\text{Disp}}$$
$$\text{where,} \quad E_{\text{disp}} = -\sum_{A,B} \frac{C_6^{AB}}{r_{AB}^6}$$

The corrections basically seek to capture the $\frac{1}{r^6}$ attraction term present within interactoin of particles. The coefficient C_6 depends on the pairs of elements A, B in consideration.

Table 3 adapted from Klimes work[83] highlights some of vdw corrections which are incorporated in current work in pursuit of better explanation of the contradictory AgAu segregation.

Table 3: Comparison of various dispersion corrections to DFT

vdw Correction	Complexity	C_6 depends on	Additional computational cost
DCACP	0	N/A	None
DFT-D2[46]	1	Constant	Small
DFT-D3[47]	2	Structure	Small
vdW-DF2 (BEEF)[48]	3	Density (calculated)	50%

DCACP stands for Dispersion corrected atom centered potentials. BEEF stands for Bayesian error estimation functional

have their own advantages for modelling different situations. DFT-D2 does give better predictions for some lattice parameters and bulk properties but it often overestimates vdW interaction in almost every system.[84] DFT-D3 is appropriate for surfaces and adsorbed species and for bulk properties.[85]

Briefly, DFT-D2 proposed by Grimme et al.[46] method is the most sim-

plest correction to DFT energies. It suffers from shortcomings such as constant corrections, diverging contribution to correction and the correction only capturing $1/r^6$ dependence.[83] DFT-D3 is the modern version developed by Grimme et al.[47] which is environment dependent and interpolates value of C_6 based on the neighbors experienced by the atom at hand. More neighbors are thought to have a squeezing effect on the central atom and it becomes less polarizable leading to decrease in C_6. BEEF is gives out nonlocal correlation energy trained via machine learning and the ensemble of functionals naturally gives out errors in energy prediction.

Each of these functionals are utilized to find the Ag segregation and Au segregation trend to investigate if including vdw force changes segregation behavior. Values obtained are plotted in Fig. 9

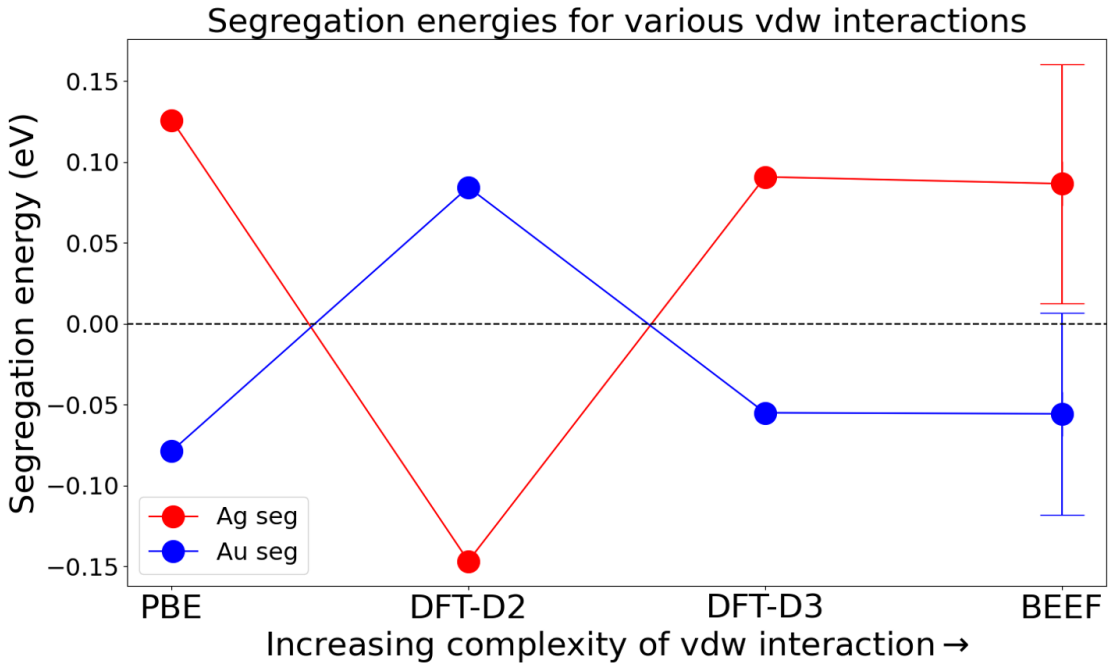

Figure 9: AgAu segregation energies for various vdw correction

It is seen from the observed values that three of the four methods employed here, predict favorable Au segregation. Only D2 method of vdw correction predicts experimentally correct Ag segregation. It can be concluded that first principles DFT calculations even after including vdw corrections suggest Au

segregation. This statement is in complete contrast to what is observed experimentally. Although this is not the first reporting of this surprising behavior. Work by Hoppe et. al.[86] compare AgAu segregation to great extent by employing various vdw correction within DFT. The authors also report Au segregation observed in their case. This mismatch observed with experiments calls for more efforts to this development and carrying out the study using more complex DFT methods.

3.8 Surface relaxation effect on Ag-Au swaps

To further investigate the mismatch of AgAu segregation, the trained Neural Network model was tested on structures with surface layers relaxed. The study employed here compares the energy predictions of atomic swaps that occur within DFT surface relaxed versus the Neural Network trained on un-relaxed structures.

A $2 \times 2 \times 5$ slab is taken and its bottom 3 layers are fixed and set to a composition of 1:1:1. Within the top two layers, 8 sites are to be occupied with either Ag or Au. This arrangement can be done in 256 ways. These arrangements are enumerated to have 256 energy unique structures. DFT energies are obtained for the first 50/256 structures, and 'swap neighbors' identified among them. Here the term swap-neighbor refer to two structures among the 256 possible, where the second structure can be obtained from the first one by swap of only one atom. Among the 1792 possible swap-neighbors, only 176 swaps are possible within the first 50 structures. The energy predictions from two cases are shown in Fig. 10

It is observed that energy of the swaps roughly lie between -0.30 eV and 0.05 eV. Neural Network predicted energies also lie within the same range. More importantly, their differences vary over a smaller range from -0.13 eV to 0.05 eV. This reduction in range of energy variation hints towards the fact that Neural Network is able to understand the underlying trend regarding

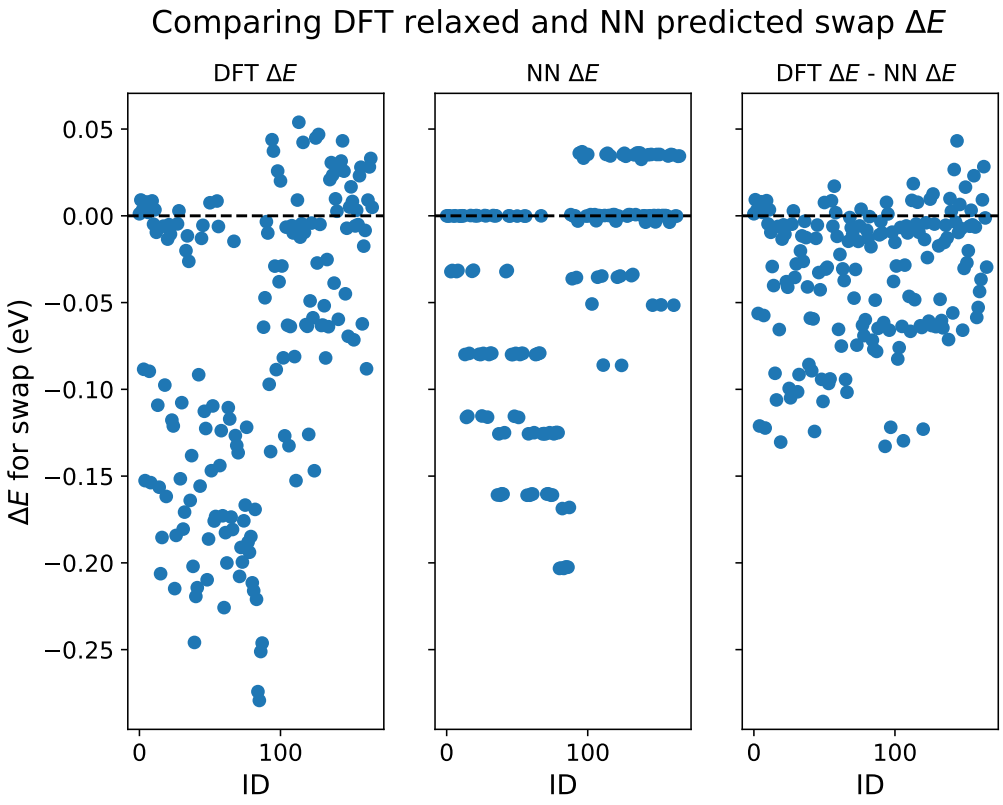

Figure 10: Neural Network performance on surface relaxed structures

relaxed structures.

Since we are interested in segregation phenomena, it is the sign of ΔE_{swap} that favors or rejects an atomic swap. We compared the sign of our Neural Network predictions to that of relaxed DFT calculations by looking at product of `sign(NN)` and `sign(DFT)`, where `sign()` is the signum function. For an atomic swap in consideration, the two should share the same sign if the product is +1. We divided the 172 possible combinations to cases which represent inter-layer exchange and intra-layer exchange. The atomic swap occurring in inter-layer exchange contribute to segregation results, while intra-layer exchanges do not.

From this analysis (refer to notebooks online for plots) it was seen that most of the inter-layer exchanges share the same sign. This points to the fact that our Neural Network although trained on unrelaxed structures, accurately captures the same sign behavior as that of relaxed DFT energy predictions. Thus, in an attempt to investigate the source of AgAu segregation mismatch, the effect of surface relaxation can be safely ignored.

3.9 TODO Segregation on 211 surface

The other common source of segregation change is that the experimentally, it's not always that we'll get FCC111 surfaces. In all of our computations, we had assumed FCC111 everywhere. To this end, we

To explore the segregation trend, we initialized a $3 \times 3 \times 5$ and studied segregation energy for each binary pair possible in CuAgAu ternary system. The results are shown in Fig. 11

The figure shows that there is no surprising change of segregation trend in any pair. For the case of Ag-Cu and Au-Cu the segregation actually gets even stronger and Ag-Au case still represents very mild segregation of Au. This study concludes that even after considering possible inclusion of FCC211 surface, the incorrect segregation trend of AgAu cannot be explained

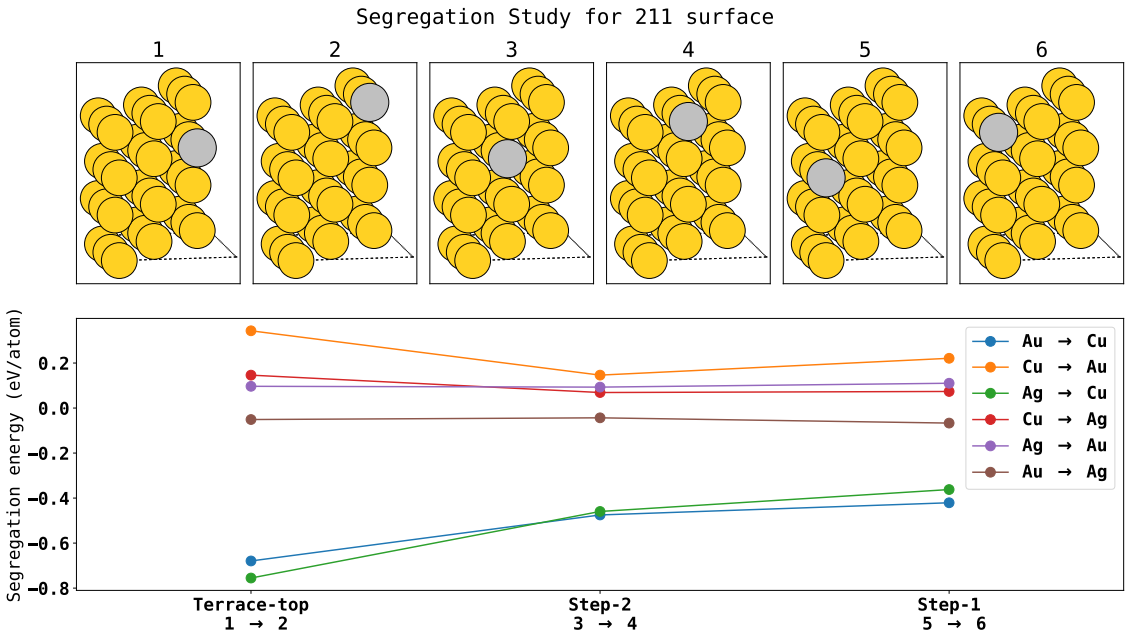

Figure 11: Segregation on 211 surface

properly.

3.10 Analytical solution to ternary surface segregation

Zhao et. al.[14] has extended the Langmuir-Mclean equations to model ternary surface segregation energies at all compositions. This model was originally developed for CuAgPd but can be extended for CuAgAu case. The reader is referred to the paper for full details. The authors provide a set of parameters for the elements: Pd, Ag, Au, Cu, Ni, Pt, and H in their previous work.[13] Briefly, segregation energy for changing compositions are calculated using formulas outlined in their previous work. Calculations are setup using these equations to obtain Fig 12 similar to Fig 7.

This analytical model does not quantitatively predict the right segregation behavior but it captures the experimental trend of Ag being surface active and Au being second surface active component. In their implementation for CuAgPd, the authors introduced an approximation in this exact model to better fit the experimental results. The approximation is included to tune

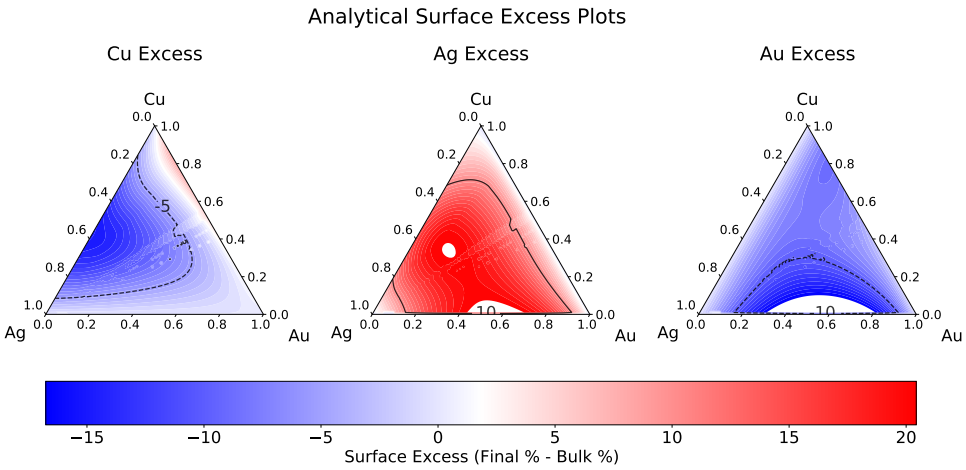

Figure 12: Analytical Surface Excess

interaction between two metals. Modifications such as these can be used to fit the experimental results to prepare a robust computational model. Authors themselves get poor extensibility to CuAgAu and it is evident from our implementation too. More work needs to go into development of this model to attain better results.

4 Conclusions

We utilized a Neural Network trained on Density Functional Theory energies to predict surface segregation in FCC111 surface of each component within CuAgAu ternary alloy. 4000 energy unique DFT calculations are used as input to the NN to capture the underlying potential energy surface. Monte Carlo simulations starting from a diverse set of compositions are started to obtain equilibrium surface composition. The trained NN provides near DFT quality values with dramatically improved speed.

It is observed that the NN achieves very high accuracy (less than 2meV/atom Mean Absolute Error) on unseen data. Surface excess predictions for all the

three elements largely match experimental results except the case of Ag-Au binary pair.

References

[1] Feng Cheng, Xiang He, Zhao-Xu Chen, and Yu-Gai Huang. Kinetic monte carlo simulation of surface segregation in Pd−Cu alloys. *Journal of Alloys and Compounds*, 648:1090–1096, 2015. doi: 10.1016/j.jallcom.2015.05.286. URL https://doi.org/10.1016/j.jallcom.2015.05.286.

[2] B. C. Han, A. Van der Ven, G. Ceder, and Bing-Joe Hwang. Surface segregation and ordering of alloy surfaces in the presence of adsorbates. *Physical Review B*, 72(20):205409, 2005. doi: 10.1103/physrevb.72.205409. URL https://doi.org/10.1103/physrevb.72.205409.

[3] John R. Kitchin, Karsten Reuter, and Matthias Scheffler. Alloy surface segregation in reactive environments: First-principles atomistic thermodynamics study of $Ag_3Pd(111)$in oxygen atmospheres. *Physical Review B*, 77(7):075437, 2008. doi: 10.1103/physrevb.77.075437. URL https://doi.org/10.1103/physrevb.77.075437.

[4] Carl A. Menning and Jingguang G. Chen. General trend for adsorbate-induced segregation of subsurface metal atoms in bimetallic surfaces. *The Journal of Chemical Physics*, 130(17):174709, 2009. doi: 10.1063/1.3125926. URL https://doi.org/10.1063/1.3125926.

[5] Donald McLean and A Maradudin. Grain boundaries in metals. *PhT*, 11(7):35, 1958.

[6] M. A. Hoffmann and P. Wynblatt. Equilibrium surface composition of ternary alloys. *Metallurgical Transactions A*, 20(2):215–223, 1989. doi: 10.1007/bf02670247. URL https://doi.org/10.1007/bf02670247.

[7] Roald Hoffmann. A chemical and theoretical way to look at bonding on surfaces. *Reviews of Modern Physics*, 60(3):601–628, 1988. doi: 10.1103/

revmodphys.60.601. URL https://doi.org/10.1103/revmodphys.60.601.

[8] M. A. Hoffmann and P. Wynblatt. Surface composition of ternary Cu−Ag−Au alloys: Part i. experimental results. *Metallurgical Transactions A*, 22(8):1833–1840, 1991. doi: 10.1007/bf02646507. URL https://doi.org/10.1007/bf02646507.

[9] M. A. Hoffmann and P. Wynblatt. Surface composition of ternary Cu−Ag−Au alloys: Part ii. a comparison of experiment with theoretical models. *Metallurgical Transactions A*, 22(8):1841–1848, 1991. doi: 10.1007/bf02646508. URL https://doi.org/10.1007/bf02646508.

[10] Brian Good, Guillermo H. Bozzolo, and Phillip B. Abel. Surface segregation in ternary alloys. *Surface Science*, 454-456:602–607, 2000. doi: 10.1016/s0039-6028(00)00283-1. URL https://doi.org/10.1016/s0039-6028(00)00283-1.

[11] P. Wynblatt and R.C. Ku. Surface energy and solute strain energy effects in surface segregation. *Surface Science*, 65(2):511–531, 1977. doi: 10.1016/0039-6028(77)90462-9. URL https://doi.org/10.1016/0039-6028(77)90462-9.

[12] R. Defay, I. Prigogine, A. Bellemans, and Everett D.H. *Surface Tension and Adsorption*. Wiley, 1966. URL https://books.google.com/books?id=teF-zAEACAAJ.

[13] Meng Zhao, Willem G. Sloof, and Amarante J. Böttger. Modelling of surface segregation for palladium alloys in vacuum and gas environments. *International Journal of Hydrogen Energy*, 43(4):2212–2223, 2018. doi: 10.1016/j.ijhydene.2017.12.039. URL https://doi.org/10.1016/j.ijhydene.2017.12.039.

[14] Meng Zhao, Johannes C. Brouwer, Willem G. Sloof, and Amarante J. Böttger. Surface segregation of ternary alloys: Effect of the interaction between solute elements. *Advanced Materials Interfaces*, 7(6):1901784, 2020. doi: 10.1002/admi.201901784. URL https://doi.org/10.1002/admi.201901784.

[15] Richard M. Lambert, Federico J. Williams, Rachael L. Cropley, and Alejandra Palermo. Heterogeneous alkene epoxidation: Past, present and future. *Journal of Molecular Catalysis A: Chemical*, 228(1-2):27–33, 2005. doi: 10.1016/j.molcata.2004.09.077. URL https://doi.org/10.1016/j.molcata.2004.09.077.

[16] Lei Cheng, Chunrong Yin, Faisal Mehmood, Bin Liu, Jeffrey Greeley, Sungsik Lee, Byeongdu Lee, Sönke Seifert., Randall E. Winans, Detre Teschner, Robert Schlögl, Stefan Vajda, and Larry A. Curtiss. Reaction mechanism for direct propylene epoxidation by alumina-supported silver aggregates: the role of the particle/support interface. *ACS Catalysis*, 4 (1):32–39, 2013. doi: 10.1021/cs4009368. URL https://doi.org/10.1021/cs4009368.

[17] J LU, J BRAVOSUAREZ, A TAKAHASHI, M HARUTA, and S OYAMA. In situ uv-vis studies of the effect of particle size on the epoxidation of ethylene and propylene on supported silver catalysts with molecular oxygen. *Journal of Catalysis*, 232(1):85–95, 2005. doi: 10.1016/j.jcat.2005.02.013. URL https://doi.org/10.1016/j.jcat.2005.02.013.

[18] Y. Lei, F. Mehmood, S. Lee, J. Greeley, B. Lee, S. Seifert, R. E. Winans, J. W. Elam, R. J. Meyer, P. C. Redfern, D. Teschner, R. Schlogl, M. J. Pellin, L. A. Curtiss, and S. Vajda. Increased silver activity for direct propylene epoxidation via subnanometer size effects. *Science*, 328(5975):

224–228, 2010. doi: 10.1126/science.1185200. URL https://doi.org/10.1126/science.1185200.

[19] Xiang Zheng, Qing Zhang, Yanglong Guo, Wangcheng Zhan, Yun Guo, Yunsong Wang, and Guanzhong Lu. Epoxidation of propylene by molecular oxygen over supported ag-cu bimetallic catalysts with low ag loading. *Journal of Molecular Catalysis A: Chemical*, 357:106–111, 2012. doi: 10.1016/j.molcata.2012.01.027. URL https://doi.org/10.1016/j.molcata.2012.01.027.

[20] Xiang Zheng, Yang-Long Guo, Yun Guo, Qing Zhang, Xiao-Hui Liu, Li Wang, Wang-Cheng Zhan, and Guan-Zhong Lu. Epoxidation of propylene by molecular oxygen over unsupported $AgCu_x$ bimetallic catalyst. *Rare Metals*, 34(7):477–490, 2015. doi: 10.1007/s12598-015-0500-y. URL https://doi.org/10.1007/s12598-015-0500-y.

[21] Xiang Feng, Xuezhi Duan, Gang Qian, Xinggui Zhou, De Chen, and Weikang Yuan. Insights into size-dependent activity and active sites of au nanoparticles supported on ts-1 for propene epoxidation with H_2 and O_2. *Journal of Catalysis*, 317:99–104, 2014. doi: 10.1016/j.jcat.2014.05.006. URL https://doi.org/10.1016/j.jcat.2014.05.006.

[22] Xiang Feng, Zhaoning Song, Yibin Liu, Xiaobo Chen, Xin Jin, Wenjuan Yan, Chaohe Yang, Jun Luo, Xinggui Zhou, and De Chen. Manipulating gold spatial location on titanium silicalite-1 to enhance the catalytic performance for direct propene epoxidation with H_2 and O_2. *ACS Catalysis*, 8(11):10649–10657, 2018. doi: 10.1021/acscatal.8b02836. URL https://doi.org/10.1021/acscatal.8b02836.

[23] Xiang Feng, Jia Yang, Xuezhi Duan, Yueqiang Cao, Bingxu Chen, Wenyao Chen, Dong Lin, Gang Qian, De Chen, Chaohe Yang, and Xinggui Zhou. Enhanced catalytic performance for propene epoxidation with

H_2 and O_2 over bimetallic Au−Ag/uncalcined titanium silicate-1 catalysts. *ACS Catalysis*, 8(9):7799–7808, 2018. doi: 10.1021/acscatal.8b01324. URL https://doi.org/10.1021/acscatal.8b01324.

[24] Werner Martienssen and Hans Warlimont. *Springer handbook of condensed matter and materials data*. Springer Science & Business Media, 2006.

[25] L. Vitos, A.V. Ruban, H.L. Skriver, and J. Kollár. The surface energy of metals. *Surface Science*, 411(1):186 – 202, 1998. ISSN 0039-6028. doi: https://doi.org/10.1016/S0039-6028(98)00363-X. URL http://www.sciencedirect.com/science/article/pii/S003960289800363X.

[26] Brian Good and Guillermo Bozzolo. Surface composition of alloys via BFS atomistic monte carlo simulation. *Surface Science*, 507-510:730–735, 2002. doi: 10.1016/s0039-6028(02)01344-4. URL https://doi.org/10.1016/s0039-6028(02)01344-4.

[27] Thomas B. Blank, Steven D. Brown, August W. Calhoun, and Douglas J. Doren. Neural network models of potential energy surfaces. *The Journal of Chemical Physics*, 103(10):4129–4137, 1995. doi: 10.1063/1.469597. URL https://doi.org/10.1063/1.469597.

[28] Jörg Behler and Michele Parrinello. Generalized neural-network representation of high-dimensional potential-energy surfaces. *Physical Review Letters*, 98(14):146401, 2007. doi: 10.1103/physrevlett.98.146401. URL https://doi.org/10.1103/physrevlett.98.146401.

[29] Tianyu Gao and John R. Kitchin. Modeling palladium surfaces with density functional theory, neural networks and molecular dynamics. *Catalysis Today*, 312:132–140, 2018. doi: 10.1016/j.cattod.2018.03.045. URL https://doi.org/10.1016/j.cattod.2018.03.045.

[30] Jacob R. Boes, Mitchell C. Groenenboom, John A. Keith, and John R. Kitchin. Neural network and reaxff comparison for Au properties. *International Journal of Quantum Chemistry*, 116(13):979–987, 2016. doi: 10.1002/qua.25115. URL https://doi.org/10.1002/qua.25115.

[31] Jacob R. Boes and John R. Kitchin. Modeling segregation on AuPd(111) surfaces with density functional theory and monte carlo simulations. *The Journal of Physical Chemistry C*, 121(6):3479–3487, 2017. doi: 10.1021/acs.jpcc.6b12752. URL https://doi.org/10.1021/acs.jpcc.6b12752.

[32] Nongnuch Artrith and Jörg Behler. High-dimensional neural network potentials for metal surfaces: a prototype study for copper. *Physical Review B*, 85(4):045439, 2012. doi: 10.1103/physrevb.85.045439. URL https://doi.org/10.1103/physrevb.85.045439.

[33] Martín Leandro Paleico and Jörg Behler. Global optimization of copper clusters at the ZnO(1010) surface using a DFT-based neural network and genetic algorithms. *The Journal of Chemical Physics*, 153 (5):054704, 2020. doi: 10.1063/5.0014876. URL https://doi.org/10.1063/5.0014876.

[34] Nongnuch Artrith, Björn Hiller, and Jörg Behler. Neural network potentials for metals and oxides - first applications to copper clusters at zinc oxide. *physica status solidi (b)*, 250(6):1191–1203, 2012. doi: 10.1002/pssb.201248370. URL https://doi.org/10.1002/pssb.201248370.

[35] Samad Hajinazar, Junping Shao, and Aleksey N. Kolmogorov. Stratified construction of neural network based interatomic models for multicomponent materials. *Physical Review B*, 95(1):014114, 2017. doi: 10.1103/physrevb.95.014114. URL https://doi.org/10.1103/physrevb.95.014114.

[36] Samad Hajinazar, Ernesto D Sandoval, Aiden J Cullo, and Aleksey N Kolmogorov. Multitribe evolutionary search for stable cupdag nanoparticles using neural network models. *Physical Chemistry Chemical Physics*, 21(17):8729–8742, 2019.

[37] Jörg Behler. First principles neural network potentials for reactive simulations of large molecular and condensed systems. *Angewandte Chemie International Edition*, 56(42):12828–12840, 2017. doi: 10.1002/anie.201703114. URL https://doi.org/10.1002/anie.201703114.

[38] G. Kresse and J. Hafner. Ab initiomolecular dynamics for liquid metals. *Physical Review B*, 47(1):558–561, 1993. doi: 10.1103/physrevb.47.558. URL https://doi.org/10.1103/physrevb.47.558.

[39] G. Kresse and J. Hafner. Ab initio molecular-dynamics simulation of the liquid-metal-amorphous-semiconductor transition in germanium. *Physical Review B*, 49(20):14251–14269, 1994. doi: 10.1103/physrevb.49.14251. URL https://doi.org/10.1103/physrevb.49.14251.

[40] G. Kresse and J. Furthmüller. Efficient iterative schemes for ab-initio total-energy calculations using a plane-wave basis set. *Physical Review B*, 54(16):11169–11186, 1996. doi: 10.1103/physrevb.54.11169. URL https://doi.org/10.1103/physrevb.54.11169.

[41] John P. Perdew, Kieron Burke, and Matthias Ernzerhof. Generalized gradient approximation made simple. *Physical Review Letters*, 77(18):3865–3868, 1996. doi: 10.1103/physrevlett.77.3865. URL https://doi.org/10.1103/physrevlett.77.3865.

[42] John P. Perdew, Kieron Burke, and Matthias Ernzerhof. Generalized gradient approximation made simple [phys. rev. lett. 77, 3865 (1996)]. *Physical Review Letters*, 78(7):1396–1396, 1997. doi: 10.1103/physrevlett.78.1396. URL https://doi.org/10.1103/physrevlett.78.1396.

[43] P. E. Blöchl. Projector augmented-wave method. *Physical Review B*, 50 (24):17953–17979, 1994. doi: 10.1103/physrevb.50.17953. URL https://doi.org/10.1103/physrevb.50.17953.

[44] G. Kresse and D. Joubert. From ultrasoft pseudopotentials to the projector augmented-wave method. *Physical Review B*, 59(3):1758–1775, 1999. doi: 10.1103/physrevb.59.1758. URL https://doi.org/10.1103/physrevb.59.1758.

[45] Hendrik J. Monkhorst and James D. Pack. Special points for brillouin-zone integrations. *Physical Review B*, 13(12):5188–5192, 1976. doi: 10.1103/physrevb.13.5188. URL https://doi.org/10.1103/physrevb.13.5188.

[46] Stefan Grimme. Semiempirical GGA-type density functional constructed with a long-range dispersion correction. *Journal of computational chemistry*, 27(15):1787–1799, 2006.

[47] Stefan Grimme, Jens Antony, Stephan Ehrlich, and Helge Krieg. A consistent and accurate ab initio parametrization of density functional dispersion correction (DFT−D) for the 94 elements H−Pu. *The Journal of Chemical Physics*, 132(15):154104, 2010. doi: 10.1063/1.3382344. URL https://doi.org/10.1063/1.3382344.

[48] Jess Wellendorff, Keld T. Lundgaard, Andreas Møgelhøj, Vivien Petzold, David D. Landis, Jens K. Nørskov, Thomas Bligaard, and Karsten W. Jacobsen. Density functionals for surface science: Exchange-correlation model development with bayesian error estimation. *Physical Review B*, 85(23):235149, 2012. doi: 10.1103/physrevb.85.235149. URL https://doi.org/10.1103/physrevb.85.235149.

[49] Jörg Behler. Atom-centered symmetry functions for constructing high-dimensional neural network potentials. *The Journal of Chemical Physics*,

134(7):074106, 2011. doi: 10.1063/1.3553717. URL https://doi.org/10.1063/1.3553717.

[50] Matthias Rupp, Alexandre Tkatchenko, Klaus-Robert Müller, and O. Anatole von Lilienfeld. Fast and accurate modeling of molecular atomization energies with machine learning. *Physical Review Letters*, 108(5):058301, 2012. doi: 10.1103/physrevlett.108.058301. URL https://doi.org/10.1103/physrevlett.108.058301.

[51] Felix Faber, Alexander Lindmaa, O. Anatole von Lilienfeld, and Rickard Armiento. Crystal structure representations for machine learning models of formation energies. *International Journal of Quantum Chemistry*, 115 (16):1094–1101, 2015. doi: 10.1002/qua.24917. URL https://doi.org/10.1002/qua.24917.

[52] Haoyan Huo and Matthias Rupp. Unified representation of molecules and crystals for machine learning, 2017.

[53] Albert P. Bartók, Risi Kondor, and Gábor Csányi. On representing chemical environments. *Physical Review B*, 87(18):184115, 2013. doi: 10.1103/physrevb.87.184115. URL https://doi.org/10.1103/physrevb.87.184115.

[54] Lauri Himanen, Marc O.J. Jäger, Eiaki V. Morooka, Filippo Federici Canova, Yashasvi S. Ranawat, David Z. Gao, Patrick Rinke, and Adam S. Foster. Dscribe: Library of descriptors for machine learning in materials science. *Computer Physics Communications*, 247:106949, 2020. doi: 10.1016/j.cpc.2019.106949. URL https://doi.org/10.1016/j.cpc.2019.106949.

[55] Adam Paszke, Sam Gross, Francisco Massa, Adam Lerer, James Bradbury, Gregory Chanan, Trevor Killeen, Zeming Lin, Natalia Gimelshein, Luca Antiga, Alban Desmaison, Andreas Kopf, Edward

Yang, Zachary DeVito, Martin Raison, Alykhan Tejani, Sasank Chilamkurthy, Benoit Steiner, Lu Fang, Junjie Bai, and Soumith Chintala. Pytorch: An imperative style, high-performance deep learning library. In H. Wallach, H. Larochelle, A. Beygelzimer, F. d'Alché-Buc, E. Fox, and R. Garnett, editors, *Advances in Neural Information Processing Systems 32*, pages 8024–8035. Curran Associates, Inc., 2019. URL http://papers.neurips.cc/paper/9015-pytorch-an-imperative-style-high-performance-deep-learning-libra pdf.

[56] Ask Hjorth Larsen, Jens Jørgen Mortensen, Jakob Blomqvist, Ivano E Castelli, Rune Christensen, Marcin Dułak, Jesper Friis, Michael N Groves, Bjørk Hammer, Cory Hargus, Eric D Hermes, Paul C Jennings, Peter Bjerre Jensen, James Kermode, John R Kitchin, Esben Leonhard Kolsbjerg, Joseph Kubal, Kristen Kaasbjerg, Steen Lysgaard, Jón Bergmann Maronsson, Tristan Maxson, Thomas Olsen, Lars Pastewka, Andrew Peterson, Carsten Rostgaard, Jakob Schiøtz, Ole Schütt, Mikkel Strange, Kristian S Thygesen, Tejs Vegge, Lasse Vilhelmsen, Michael Walter, Zhenhua Zeng, and Karsten W Jacobsen. The atomic simulation environment—a python library for working with atoms. *Journal of Physics: Condensed Matter*, 29(27):273002, 2017. URL http://stacks.iop.org/0953-8984/29/i=27/a=273002.

[57] S. R. Bahn and K. W. Jacobsen. An object-oriented scripting interface to a legacy electronic structure code. *Comput. Sci. Eng.*, 4(3):56–66, MAY-JUN 2002. ISSN 1521-9615. doi: 10.1109/5992.998641.

[58] Carson Sievert. *Interactive Web-Based Data Visualization with R, plotly, and shiny*. Chapman and Hall/CRC, 2020. ISBN 9781138331457. URL https://plotly-r.com.

[59] G. Tréglia, B. Legrand, F. Ducastelle, A. Saúl, C. Gallis, I. Meunier,

C. Mottet, and A. Senhaji. Alloy surfaces: Segregation, reconstruction and phase transitions. *Computational Materials Science*, 15(2):196–235, 1999. doi: 10.1016/s0927-0256(99)00004-x. URL https://doi.org/10.1016/s0927-0256(99)00004-x.

[60] J. Y. Wang, J. du Plessis, J. J. Terblans, and G. N. van Wyk. Equilibrium surface segregation of silver to the low-index surfaces of a copper single crystal. *Surface and Interface Analysis*, 28(1):73–76, 1999. doi: 10.1002/(sici)1096-9918(199908)28:1<73::aid-sia621>3.0.co;2-e. URL https://doi.org/10.1002/(sici)1096-9918(199908)28:1<73::aid-sia621>3.0.co;2-e.

[61] J.Y Wang, J du Plessis, J.J Terblans, and G.N van Wyk. The discontinuous surface transition in the Cu(111)(Ag) binary segregating system. *Surface Science*, 419(2-3):197–206, 1999. doi: 10.1016/s0039-6028(98)00790-0. URL https://doi.org/10.1016/s0039-6028(98)00790-0.

[62] A. V. Ruban, H. L. Skriver, and J. K. Nørskov. Surface segregation energies in transition-metal alloys. *Physical Review B*, 59(24):15990–16000, 1999. doi: 10.1103/physrevb.59.15990. URL https://doi.org/10.1103/physrevb.59.15990.

[63] V.I. Razumovskiy, S.V. Divinski, and L. Romaner. Solute segregation in Cu: DFT vs. experiment. *Acta Materialia*, 147(nil):122–132, 2018. doi: 10.1016/j.actamat.2018.01.011. URL https://doi.org/10.1016/j.actamat.2018.01.011.

[64] Daniela S. Mainardi and Perla B. Balbuena. Surface segregation in bimetallic nanoclusters: Geometric and thermodynamic effects. *International Journal of Quantum Chemistry*, 85(4-5):580–591, 2001. doi: 10.1002/qua.1524. URL https://doi.org/10.1002/qua.1524.

[65] Edgar Völker, Federico J. Williams, Ernesto J. Calvo, Timo Jacob, and David J. Schiffrin. O_2 induced cu surface segregation in Au−Cu alloys studied by angle resolved XPS and DFT modelling. *Physical Chemistry Chemical Physics*, 14(20):7448, 2012. doi: 10.1039/c2cp40565b. URL https://doi.org/10.1039/c2cp40565b.

[66] Chunrong Yin, Zhitao Guo, and Andrew J. Gellman. Surface segregation across ternary alloy composition space: $Cu_xAu_yPd_{1-x-y}$. *The Journal of Physical Chemistry C*, page acs.jpcc.0c02058, 2020. doi: 10.1021/acs.jpcc.0c02058. URL https://doi.org/10.1021/acs.jpcc.0c02058.

[67] M A Vasiliev. Surface effects of ordering in binary alloys. *Journal of Physics D: Applied Physics*, 30(22):3037–3070, 1997. doi: 10.1088/0022-3727/30/22/002. URL https://doi.org/10.1088/0022-3727/30/22/002.

[68] S. Fain and J. McDavid. Work-function variation with alloy composition: Ag−Au. *Physical Review B*, 9(12):5099–5107, 1974. doi: 10.1103/physrevb.9.5099. URL https://doi.org/10.1103/physrevb.9.5099.

[69] R Bouwman, L.H Toneman, M.A.M Boersma, and R.A Van Santen. Surface enrichment in AgAu alloys. *Surface Science*, 59(1):72–82, 1976. doi: 10.1016/0039-6028(76)90292-2. URL https://doi.org/10.1016/0039-6028(76)90292-2.

[70] K. Meinel, M. Klaua, and H. Bethge. Segregation and sputter effects on perfectly smooth (111) and (100) surfaces of auag alloys studied by aes. *Physica Status Solidi (a)*, 106(1):133–144, 1988. doi: 10.1002/pssa.2211060117. URL https://doi.org/10.1002/pssa.2211060117.

[71] S.H Overbury and G.A Somorjai. The surface composition of the silver-gold system by auger electron spectroscopy. *Surface Science*, 55(1):209–

226, 1976. doi: 10.1016/0039-6028(76)90385-x. URL https://doi.org/10.1016/0039-6028(76)90385-x.

[72] T.S. King and R.G. Donnelly. Surface compositions and composition profiles of AgAu (100), (110), and (111) surfaces determined quantitatively by auger electron spectroscopy. *Surface Science*, 151(2-3):374–399, 1985. doi: 10.1016/0039-6028(85)90382-6. URL https://doi.org/10.1016/0039-6028(85)90382-6.

[73] G.C Nelson. Determination of the surface versus bulk composition of silver-gold alloys by low energy ion scattering spectroscopy. *Surface Science*, 59(1):310–314, 1976. doi: 10.1016/0039-6028(76)90310-1. URL https://doi.org/10.1016/0039-6028(76)90310-1.

[74] M. J. Kelley, D. G. Swartzfager, and V. S. Sundaram. Surface segregation in the Ag−Au and Pt−Cu systems. *Journal of Vacuum Science and Technology*, 16(2):664–667, 1979. doi: 10.1116/1.570052. URL https://doi.org/10.1116/1.570052.

[75] G.N. Derry and R. Wan. Comparison of surface structure and segregation in AgAu and NiPd alloys. *Surface Science*, 566-568(nil):862–868, 2004. doi: 10.1016/j.susc.2004.06.022. URL https://doi.org/10.1016/j.susc.2004.06.022.

[76] Guillermo Bozzolo, Jorge E. Garcés, and Gregory N. Derry. Atomistic modeling of segregation and bulk ordering in ag-au alloys. *Surface Science*, 601(9):2038–2046, 2007. doi: 10.1016/j.susc.2007.02.035. URL https://doi.org/10.1016/j.susc.2007.02.035.

[77] Lei Deng, Wangyu Hu, Huiqiu Deng, Shifang Xiao, and Jianfeng Tang. Au−Ag bimetallic nanoparticles: Surface segregation and atomic-scale structure. *The Journal of Physical Chemistry C*, 115(23):11355–11363,

2011. doi: 10.1021/jp200642d. URL https://doi.org/10.1021/jp200642d.

[78] Fuyi Chen and Roy L. Johnston. Charge transfer driven surface segregation of gold atoms in 13-atom Au−Ag nanoalloys and its relevance to their structural, optical and electronic properties. *Acta Materialia*, 56(10):2374–2380, 2008. doi: 10.1016/j.actamat.2008.01.048. URL https://doi.org/10.1016/j.actamat.2008.01.048.

[79] Lauro Oliver Paz-Borbón, Roy L. Johnston, Giovanni Barcaro, and Alessandro Fortunelli. Structural motifs, mixing, and segregation effects in 38-atom binary clusters. *The Journal of Chemical Physics*, 128 (13):134517, 2008. doi: 10.1063/1.2897435. URL https://doi.org/10.1063/1.2897435.

[80] A. L. Gould, C. J. Heard, A. J. Logsdail, and C. R. A. Catlow. Segregation effects on the properties of (AuAg)147. *Phys. Chem. Chem. Phys.*, 16(39):21049–21061, 2014. doi: 10.1039/c4cp00753k. URL https://doi.org/10.1039/c4cp00753k.

[81] Vlasta Bonačić-Koutecký, Jaroslav Burda, Roland Mitrić, Maofa Ge, Giuseppe Zampella, and Piercarlo Fantucci. Density functional study of structural and electronic properties of bimetallic silver-gold clusters: Comparison with pure gold and silver clusters. *The Journal of Chemical Physics*, 117(7):3120–3131, 2002. doi: 10.1063/1.1492800. URL https://doi.org/10.1063/1.1492800.

[82] J. J. Rehr, E. Zaremba, and W. Kohn. Van der waals forces in the noble metals. *Physical Review B*, 12(6):2062–2066, 1975. doi: 10.1103/physrevb.12.2062. URL https://doi.org/10.1103/physrevb.12.2062.

[83] Jiří Klimeš and Angelos Michaelides. Perspective: Advances and challenges in treating van der waals dispersion forces in density functional theory. *The Journal of Chemical Physics*, 137(12):120901, 2012. doi: 10.1063/1.4754130. URL https://doi.org/10.1063/1.4754130.

[84] Tomas Bučko, Jurgen Hafner, Sébastien Lebegue, and János G Angyán. Improved description of the structure of molecular and layered crystals: ab initio DFT calculations with van der waals corrections. *The Journal of Physical Chemistry A*, 114(43):11814–11824, 2010.

[85] Werner Reckien, Florian Janetzko, Michael F. Peintinger, and Thomas Bredow. Implementation of empirical dispersion corrections to density functional theory for periodic systems. *Journal of Computational Chemistry*, 33(25):2023–2031, 2012. doi: 10.1002/jcc.23037. URL https://doi.org/10.1002/jcc.23037.

[86] Sandra Hoppe and Stefan Müller. A first principles study on the electronic origins of silver segregation at the Ag−Au (111) surface. *Journal of Applied Physics*, 122(23):235303, 2017. doi: 10.1063/1.5017959. URL https://doi.org/10.1063/1.5017959.